RESEARCH ARTICLE | JULY 14 2023

# Viscosity impact on 3D non-linear MHD simulations of RFP fusion plasmas

N. Vivenzi ; M. Veranda ; D. Bonfiglio ; S. Cappello



*Phys. Plasmas* 30, 072304 (2023)
https://doi.org/10.1063/5.0150255

# Viscosity impact on 3D non-linear MHD simulations of RFP fusion plasmas

Cite as: Phys. Plasmas **30**, 072304 (2023); doi: 10.1063/5.0150255
Submitted: 13 March 2023 · Accepted: 21 June 2023 ·
Published Online: 14 July 2023



N. Vivenzi,[1,2,a)] M. Veranda,[1,3] D. Bonfiglio,[1,3] and S. Cappello[1,3]

## AFFILIATIONS

[1]Consorzio RFX (CNR, ENEA, INFN, Università degli Studi di Padova, Acciaierie Venete SpA), C.so Stati Uniti 4, 35127 Padova, Italy
[2]CRF-University of Padova, C.so Stati Uniti 4, 35127 Padova, Italy
[3]CNR-ISTP Padova, C.so Stati Uniti 4, 35127 Padova, Italy

[a)]**Author to whom correspondence should be addressed:** nicholas.vivenzi@studenti.unipd.it

## ABSTRACT

Several studies pointed out the joint role of resistivity $\eta$ and viscosity $\nu$ in determining the dynamics and the emergence of helical regimes of reversed-field pinch (RFP) plasmas. In this framework, the self-consistent time evolution of the $\eta$ and $\nu$ coefficients still lacks of a fully satisfying modeling, being constrained by many approximations. In this work, the hypothesis of a flat viscosity profile is relaxed: A viscosity profile inspired by the Braginskii perpendicular viscosity is implemented in the code. This choice is motivated by the fact that the magnetohydrodynamics field instabilities relevant for the RFP configuration dynamics (resistive-kink/tearing modes) are active in the direction perpendicular to the magnetic field. Such a non-monotonous profile causes a localized damping of plasma flow in the regions, where the viscosity is stronger, close to the plasma edge. This results in the reduction of the flow shear, in turn allowing the enhancement of edge magnetic field modes amplitude. The impact on the magnetic topology and on connection length to the wall is also analyzed.





## I. INTRODUCTION

In fusion research, 3D non-linear visco-resistive magnetohydrodynamics (MHD) represents a fundamental tool in modeling the dynamics of toroidal pinches,[1] with reference to both the configurations: tokamak and reversed-field pinch, RFP. Fundamental results have been obtained exploiting the RFP configuration, which represents a toroidal magnetic configuration for the confinement of fusion plasmas, characterized by relatively high values of the plasma current with respect to magnetic flux.[2] An important feature of the RFP is the plasma helical self-organization,[3] characterized by the dominance of a single mode over all the magnetic field spectrum that gives its dominant helical twist to the whole plasma column. This condition, which was originally observed at high visco-resistive dissipation in numerical simulations,[4,5] is realized in the experiments during high plasma current operations ($I_p \geq 1$MA on RFX-mod device), and it is accompanied by the formation of transport barrier and the improvement of plasma confinement.[3,6–8]

In the last few decades, non-linear visco-resistive MHD modeling has played a key role in describing the plasma helical self-organizing process (see Sec. II). In particular, the transport coefficients of the model (resistivity and viscosity) determine, together with the application of proper plasma boundary conditions, the possible occurrence of helical states.[9,10]

In the context of visco-resistive MHD, the joint role of resistivity and viscosity has been pointed out in several works, see, e.g., Refs. 11–13, with particular reference to the occurrence of steady state helical solutions. The toroidal geometry has also been proven to play an important role in this framework (see, e.g., Refs. 14 and 15).

Despite the importance of using the proper transport coefficients to describe RFP regimes, see Refs. 6, 16, and 17, no unique consensus still exists about the evaluation of such coefficients. The existence of an important anomaly between the classical transport prediction by Braginskii[18] and the experimental measurements is pointed out, for both the resistivity[19,20] and the viscosity.[21–26]

In the case of resistivity, in Refs. 27 and 28, a remarkable agreement is shown between the Spitzer estimate (coinciding with the Braginskii formula) and the experimental measurements of the resistivity during magnetic reconnection experiments in collisional regime. However, in Ref. 19, the effective resistivity (and the consequent toroidal loop voltage) is shown to deviate significantly from the classical estimate because of the dynamo action. In addition, a recent work[20] has pointed out the need for an order of magnitude anomaly of the resistivity in order to obtain a quantitative agreement between the

linear resistive MHD model predictions and resonant modes growth rate measurements on the EXTRAP T2R reversed-field pinch device.

For the viscosity, the uncertainty in the coefficient estimate is even larger,[29] and the existence of a two orders of magnitude anomaly between the Braginskii estimate and the experimental measurements is confirmed by recent studies.[21–26]

In non-linear MHD codes, simplified expressions are commonly used to model the transport coefficients profiles. In particular, the M3D,[30] and PIXIE3D[31] codes usually adopt a Spitzer-like dependence of the resistivity profile ($\eta(r) \propto T_e^{-3/2}$) and a uniform profile for the viscosity, while in the non-linear extended code JOREK,[32] in addition to the Spitzer-like resistivity, the viscosity term is split into two contributions: the parallel (spatially constant) and the perpendicular (whose profile is evolved as the resistivity one, to maintain a constant ratio between the two coefficients over the whole plasma volume). In the non-linear spectral code SpeCyl,[33] the one considered in this paper, the present modeling of transport coefficients profiles is rather simple, considering a uniform, scalar viscosity profile, and no evolution in time for both resistivity and viscosity. At the current state of knowledge, the relaxation of such assumptions in MHD simulations deserves further studies (see, e.g., Ref. 34, where non-uniform transport coefficients are introduced for both tokamak and RFP configurations, and Ref. 35, where the effects of non-uniform profiles on $m = 0$ modes stability are studied), which are carried out in this work.

The aim of this paper is to test the effects on the plasma dynamics and on the magnetic topology of a non-uniform viscosity profile, inspired by the Braginskii transport theory and by simplified radial profiles of plasma measurable quantities. We show that a Braginskii-like viscosity profile causes a shear flow suppression, allowing the enhancement of edge magnetic field modes amplitude. This recalls a well-known mechanism of microturbulence suppression induced by edge shear flow.[36]

In Sec. II, the SpeCyl code for 3D non-linear visco-resistive MHD simulations is introduced, discussing: the approximations of the model, the equations solved, and the numerical scheme adopted by the code. A brief summary of the main advancements made in MHD modeling using the SpeCyl code is also provided.

In Sec. III, we discuss the choice of the viscosity profiles studied in this work, qualitatively describing the different viscosity values as the radial position in the cylinder varies.

In Sec. IV, the simulations results are analyzed in terms of the plasma dynamics. In particular, we firstly analyzed the temporal evolution and the spectra of both the kinetic and the magnetic energy, followed by the poloidal flow, the poloidal shear flow, and the radial magnetic field instabilities at selected radial positions. This has allowed us to draw a basic picture of interplay between viscosity coefficient, the sheared velocity, and the magnetic field, where the tested viscosity profile is shown to damp the velocity and the velocity shear, allowing a slight enhancement of the magnetic field instabilities.

In Sec. V, the profile effects on the viscosity anomaly is described, showing that a Braginskii-like viscosity profile could contribute in reducing the anomaly of about a factor three.

In Sec. VI, the simulations results are analyzed in terms of the magnetic topology. In particular, the Poincaré plots and the contourplots of the connection length for selected time instants are described, showing that the introduction of a perpendicular Braginskii profile decreases the average value of the connection length, which can be interpreted as a sign of an increased activity of the $m = 1$ intermediate resonant modes.

Conclusions and final remarks follow in Sec. VII.

## II. SPECYL VISCO-RESISTIVE MHD SIMULATIONS

This section is devoted to introducing the 3D non-linear visco-resistive MHD model and to presenting the SpeCyl code, the numerical tool used to study reversed-field pinch fusion plasmas in this work. The model is derived from single fluid MHD equations, assuming a constant and uniform mass density[4,37] and neglecting the effects introduced by the pressure gradient in the equation of motion. As highlighted in Ref. 38, models adopting similar approximations have been extensively used for compressible laboratory plasmas, capturing major physical effects observed in experiments (see, for example, Refs. 39–47). Moreover, focusing on current driven instabilities, we are much more interested in the effects introduced by the Lorentz force term and then in those introduced by the pressure gradient. According to this simplification, the latter term is neglected.[48] In this case, only the electromagnetic Lorentz force and the momentum diffusion term (modulated by the viscosity) contribute in determining the plasma dynamics.

The model consists of the following equations, written in Alfvénic units:

$$\rho_0\left(\frac{\partial \mathbf{v}}{\partial t} + (\mathbf{v}\cdot\nabla)\mathbf{v}\right) = \mathbf{j}\times\mathbf{B} + \rho_0\nu\nabla^2\mathbf{v}, \tag{1}$$

$$\frac{\partial \mathbf{B}}{\partial t} = \nabla\times(\mathbf{v}\times\mathbf{B}) - \nabla\times(\eta\mathbf{j}), \tag{2}$$

$$\nabla\cdot\mathbf{B} = 0, \tag{3}$$

$$\mathbf{j} = \nabla\times\mathbf{B}, \tag{4}$$

where space, time, and magnetic field are normalized, respectively, to plasma minor radius $a$, Alfvén time $\tau_A$, and on-axis magnetic field $B_0$, while $\rho_0$ represents the constant and uniform mass density. In these units, resistivity and viscosity (that represent the transport coefficients of the model) are expressed naturally as the inverse of the Lundquist number $\eta = \tau_r/\tau_A = S^{-1}$ and of the viscous Lundquist number $\nu = \tau_\nu/\tau_A = M^{-1}$. Even if Eq. (1) should be modified by the introduction of a non-uniform viscosity, we will consider the additional terms negligible in the context of this paper, see the Appendix, maintaining the current formulation of the equations for this sensitivity study.

SpeCyl[33] solves the equations of model (1–4) in cylindrical geometry, adopting a semi-implicit temporal advance scheme and exploiting a spectral formulation in the axial and azimuthal coordinates and a finite differences scheme in the radial one.

This code has successfully undergone a cross-benchmark nonlinear verification study[49] with the 3D finite volume MHD code PIXIE3D.[31] With a proper change of coordinates $(t, \mathbf{v}) \rightarrow (\bar{t} = \sqrt{\eta/\nu}\,t, \bar{\mathbf{v}} = \sqrt{\nu/\eta}\,\mathbf{v})$ and the introduction of the Prandtl $P = \nu/\eta$ and the Hartmann numbers $H = 1/\sqrt{\eta\nu}$, the plasma dynamics (1)–(4) is shown to depend only on the latter dimensionless coefficient, if the inertia term in Eq. (1) becomes negligible.[16] Therefore, the Hartmann number turns out to be the ruling parameter of the MHD activity,[10] highlighting the joint role of both resistivity and viscosity in determining the plasma dynamics and the need for an experimental evaluation of both the transport coefficients. More

recently, the predictions of the model have reached a good level of agreement with the RFX-mod data, being able to describe both the helical twist[9] and the intensity of the perturbed mode[38] of helical states, exploiting the introduction of non-ideal magnetic field boundary conditions. The latter consists of imposing an edge non-zero radial magnetic field, mimicking edge radial magnetic field, also known as magnetic perturbation (MP). This is essential to reproduce a helically self-organized regime even at low dissipation, the so-called quasi-single helicity regime, characterized by periodic repetition of an ordered phase, suddenly interrupted by reconnection events (crashes). No slip boundary conditions are considered for the axial and the azimuthal components of the velocity [$v_z(a) = 0$, $v_\theta(a) = 0$], while an inward finite pinch velocity is assumed only for the $m = 0$, $n = 0$ radial component, caused by the electric and magnetic field interaction and determined by the Ohm's law: $v_r^{0,0}(a) = ((E_0 \mathbf{e}_z \times \mathbf{B}) \cdot \mathbf{e}_r / B^2)^{0,0}$. This is qualitatively in agreement with the experimental picture (characterized by an almost uniform, constant density), where the inward radial pinch velocity and the influx of particles coming from the wall can be thought as particle source terms that contribute in the continuity equation to the balance of the flow divergence. The quantitative balance of these terms in the MHD modeling framework is beyond the scope of this paper. The transport coefficients ($\eta$, $\nu$) have been considered to be constant in time. In the past, the same profile [Eq. (5a)] was considered for both the resistivity and the viscosity, to maintain a uniform value of the Prandtl number on the plasma volume.[50] However, in the most recent SpeCyl simulations, a simple radial profile is commonly assumed for both resistivity $\eta(r)$ and viscosity $\nu(r)$,

$$\eta(r) = \eta_0(1 + 20r^{10}), \tag{5a}$$

$$\nu(r) = \nu_0. \tag{5b}$$

More precisely, the resistivity profile expression is derived applying the Spitzer resistivity formula ($\eta \propto T_e^{-3/2}$)[51] to typical RFX-mod electron temperature profiles, while the viscosity profile is preliminary assumed to be uniform. In this regard, the setting of a Braginskii-like viscosity profile (inspired by simplified radial profiles of temperature, density, and magnetic field in RFX-mod plasmas) is going to be discussed in Sec. III, with the aim of describing its effects on the plasma dynamics and the magnetic topology with respect to flat profile in Eq. (5b), the mostly adopted so far.

## III. SIMULATION SETTINGS

In this section, we describe the SpeCyl simulations considered for this study.

The settings common to all the three simulations are the absolute on-axis values of the resistivity: $\eta_0 = 10^{-6}$ and viscosity: $\nu_0 = 10^{-4}$, and the resistivity profile, chosen according to Eq. (5a). We focus, presently, on the case of ideal boundary conditions simulations, leading to a multiple helicity regime, that is experimentally observed in low current RFP discharges. The Fourier spectrum selected for this analysis is reported in Table I for both the azimuthal (poloidal) wave number $m$ and axial (toroidal) wave number $n$. We recall that the convention adopted in the Fourier decomposition is $\exp[i(m\theta + nz/R_0)]$. The modes spectrum shown in this study was selected after a convergence study (see Ref. 33) and includes also non-resonant modes (e.g., $m = 1$, $-7 < n < 0$). As we will see from Fig. 2, the number of selected modes is adequate for the study.

**TABLE I.** Details of the Fourier spectrum considered in the SpeCyl simulations analyzed for the azimuthal (poloidal) wave number $m$ and axial (toroidal) wave number $n$. 225 Fourier modes are considered, in addition to the axisymmetric component (0, 0).

| $m$ | 0 | 1 | 2 | 3 | 4 |
|---|---|---|---|---|---|
| $n$ | $[-25; 0]$ | $[-55; 9]$ | $[-50; -6]$ | $[-60; -16]$ | $[-70; -26]$ |

Although many radial dependencies for the viscosity were considered, in this paper, we compare the three more significant simulations (only differing for the viscosity profile considered), as shown in Fig. 1(a).

The first profile is the flat profile $\nu_{\text{flat}}(r) = \nu_0$, which represents the reference case of study in SpeCyl simulations so far.[9,38]

The second profile is inspired by the perpendicular Braginskii viscosity coefficient evaluated on experimental-like plasma parameters profiles: $\nu_{Brag,\perp}(r) = \nu_0(1 + 20r^3 \cos(1.6r))$.[18] Some remarks are needed in order to justify this choice. First of all, we mention that RFP dynamics are determined by magnetic instabilities and fluid convection, which both develop in the direction perpendicular to the magnetic field. In a recent study, Ref. 52, different viscosity coefficients have been estimated according to the main theories of transport and we have compared the trends of the amplitudes of magnetic field

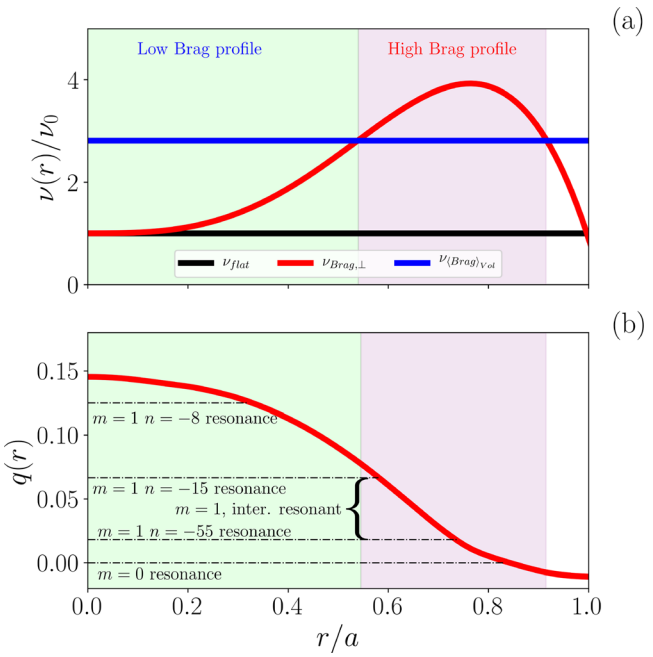


**FIG. 1.** (a) Comparison of viscosity profiles set in SpeCyl simulations: the flat viscosity profile $\nu_{\text{flat}}$ (black), the profile that comes from using the perpendicular Braginskii viscosity $\nu_{\text{Brag},\perp}$ (red), and the flat profile with the same volume average viscosity of the Braginskii one, $\nu_{\langle\text{Brag}\rangle_{\text{Vol}}}$ (blue). (b) Safety factor profile of a RFP plasma, with the main instability resonances marked with horizontal lines. Two different regions are highlighted: the region where the Braginskii viscosity profile is lower than its volume average ($\nu_{\text{Brag},\perp} < \nu_{\langle\text{Brag}\rangle_{\text{Vol}}}$, in green) and the one where it is higher ($\nu_{\text{Brag},\perp} > \nu_{\langle\text{Brag}\rangle_{\text{Vol}}}$, in purple). In the first region, the resonances of the $m = 1$, $-14 \leq n \leq -7$ are located, while in the second, the $m = 0$ and $m = 1$, $-55 \leq n \leq -15$ modes resonances are located.

instabilities at the edge as a function of the Hartmann number between SpeCyl simulations and RFX-mod experimental data. We have preliminary shown that the parallel Braginskii viscosity, which is larger by about seven orders of magnitude than the perpendicular one, is the one that gives the worst quality fit. For this reason, we identified the parallel viscosity estimate as not suitable for an optimal comparison between SpeCyl simulations and RFX-mod data. On the contrary, even if it is not the largest among the possible viscosity estimates, the perpendicular Braginskii coefficient with a suitably anomaly factor represents the contribution to the plasma viscosity which provides the best agreement. The perpendicular Braginskii viscosity (in its dimensionless form, i.e., the reciprocal of the viscous Lundquist number) is expressed as a function of the plasma measurable parameters,

$$\nu_{Brag,\perp} = \frac{1}{M_{Brag,\perp}} \propto \frac{\gamma Z^{1/2} \ln \Lambda}{a} \frac{n^{3/2}}{B^3 T_i^{1/2}}, \tag{6}$$

where the mass number $\gamma$, the effective charge $Z$, the Coulomb Logarithm, and the plasma minor radius $a$ are considered constant; a polynomial profile is considered for the density and the temperature: $n(r)/n_0, T(r)/T_0 = 1 - r^5$. This choice is motivated by considering basic analytical expressions resembling typical RFX-mod profiles[53] for the main plasma measurable quantities. The values and the profile of the viscosity are not evolved self-consistently by the code. The Bessel function model is considered as simple approximation[54] for the magnetic field modulus.

The third profile is a flat profile (as the first one) but with a different central value, exactly amounting to the volume average viscosity of $\nu_{Brag,\perp}(r)$: $\nu_{\langle Brag\rangle_{Vol}}(r) \sim 2.82\nu_0$, which allows the study of the effects purely due to the profile, by comparison with the simulation based on Eq. (6).

The introduction of Braginskii-like viscosity profiles does not modify significantly the axisymmetric component of the magnetic fields. In Fig. 1(b), the safety factor profile of the simulations is shown, calculated using the time average of the $m = 0$, $n = 0$ magnetic field, $q(r) = (r\langle B_z^{0,0}(r)\rangle_t)/(R_0\langle B_\theta^{0,0}(r)\rangle_t)$.

We preliminary observe that in the core region (highlighted in green), where the Braginskii perpendicular viscosity profile is lower than its volume average value: $\nu_{Brag,\perp} < \nu_{\langle Brag\rangle_{Vol}}$, the modes $m = 1$, $-14 \le n \le -7$ resonate. On the contrary, in the external region (highlighted in purple), the Braginskii viscosity profile is higher than its volume average value $\nu_{Brag,\perp} > \nu_{\langle Brag\rangle_{Vol}}$. This is the region where the reversal of the toroidal magnetic field occurs (and consequently the resonance of the $m = 0$ modes) and the resonance of the $m = 1$, $n \le -15$ modes is located. The approach of considering a viscosity higher in the external region is followed also in Ref. 35 with the aim of studying the excitation of $m = 0$ modes during the sawtooth crash. In the present study, the viscosity peak in the external region is a result of the application of the Braginskii theory upon reasonable profile estimates.

## IV. BRAGINSKII-LIKE VISCOSITY PROFILE: EFFECTS ON THE DYNAMICS

In this section, the effects of Braginskii-like viscosity profiles on the plasma dynamics are studied, firstly focusing on the volume integral quantities (kinetic and magnetic energy) and then on the velocity and magnetic fields, which instead display also a dependence on spatial coordinates. Since in any fluid model, the viscosity coefficient directly acts on the velocity field, see Eq. (1), and then, it influences the other quantities (like the magnetic field) by means of the coupled equations [Eq. (2) in the present model], we will proceed giving priority to the velocity related quantities (like the kinetic energy $W_k$) and then analyzing the magnetic field related ones (like the magnetic energy $W_M$).

As a preliminary study, the spectra of both the kinetic and the magnetic energy are shown in Fig. 2, for the $m = 0$ and the $m = 1$ modes and for any viscosity profile analyzed. The energy time average is calculated (for each mode) over the simulation time interval. The energies of $m = 0$ modes display an almost monotonously increasing trend as $n$ is increased, while, for the $m = 1$ modes, a maximum point is displayed for $n = -8$. The spectrum tails, which are small with respect to the peak values, show that the number of harmonics analyzed is adequate for this study. For the sake of completeness, we also plot in Fig. 3, the values of all the harmonics, where the general trend of kinetic components decreases and of magnetic components increase can be observed on the global values, when a volume increase in the viscosity is applied.

To investigate the purely effect of the viscosity profile, in Fig. 4, the time evolution of the kinetic and the magnetic energy is compared for the three viscosity profiles: $\nu_{\text{flat}}$, $\nu_{Brag,\perp}$, and $\nu_{\langle Brag\rangle_{Vol}}$. Considering the shape of the profiles and the safety factor (Fig. 1), three contributions are highlighted: the $m = 1$ "core resonant" modes $-14 \le n \le -7$, the average of the $m = 1$ "intermediate resonant" modes $(-55 \le n \le -15)$, and the average of the $m = 0$ secondary modes $(-25 \le n \le -1)$. The choice of the $m = 1$ intermediate resonant modes is suggested by the shape of the $\nu_{Brag,\perp}$ profile. These modes are in fact those which resonates in correspondence of the region, where the Braginskii perpendicular profile is higher than its volume average.

We preliminary observe that the dynamics is not qualitatively altered by the viscosity profile. However, we observe that the Braginskii-like viscosity profiles $\nu_{Brag,\perp}$ and $\nu_{\langle Brag\rangle_{Vol}}$ cause a reduction of the kinetic energy and a slight enhancement of the magnetic energy: This is consistent with an effect of plasma flows counteracting the growth of magnetic perturbations.[55] To make a more quantitative comparison, the numerical values of the time average of the energy are considered in Fig. 5, where we also compute the average of all the modes except the $(m, n) = (0, 0)$, showing that a volume average increase in the viscosity of about a factor three causes the halving of the kinetic energy and a 30% increase in the magnetic energy of the MHD modes. The energy related to the axisymmetric part of the velocity field is reduced by almost 20%, while the axisymmetric part of the magnetic field is unaffected by the new profiles.

In Fig. 6, the spectrum ratios for the kinetic (a)–(c) and the magnetic energy (d)–(f) are shown with the aim of analyzing the effect of the new Braginskii-like profile with respect to the flat one (a) and (d). The spectrum ratios are computed according to the following expressions:

$$\frac{\langle W_{m,n}^{\nu_{Brag,\perp}}\rangle_t}{\langle W_{m,n}^{\nu_{\text{flat}}}\rangle_t}, \quad \frac{\langle W_{m,n}^{\nu_{\langle Brag\rangle_{Vol}}}\rangle_t}{\langle W_{m,n}^{\nu_{\text{flat}}}\rangle_t}, \quad \frac{\langle W_{m,n}^{\nu_{Brag,\perp}}\rangle_t}{\langle W_{m,n}^{\nu_{\langle Brag\rangle_{Vol}}}\rangle_t},$$

being $W = W_k, W_M$, for the harmonics with wave numbers $m = 1$, $-55 \le n \le 9$, and $m = 0$, $-25 \le n \le -1$, which represents all the $m = 0$ and $m = 1$ modes computed by the code. The global damping

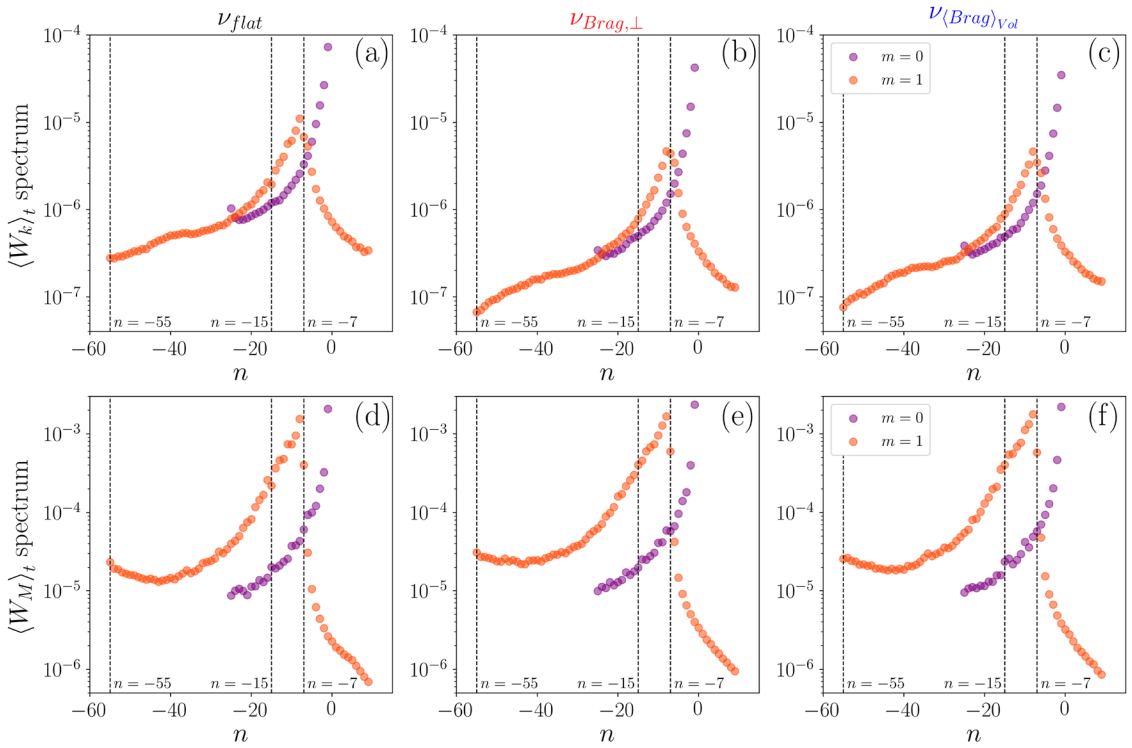


**FIG. 2.** Kinetic and magnetic energy spectrum comparison for SpeCyl simulations distinguished by the viscosity profile: $\nu_{flat}$ (a) and (d), $\nu_{Brag,\perp}$ (b) and (e), and $\nu_{\langle Brag\rangle_{Vol}}$ (c) and (f). The time average is computed for each mode: $m = 0$, $-25 \le n \le -1$ (in purple) and $m = 1$, $-55 \le n \le 9$ (in orange). For both kinetic $W_k$ (a)–(c) and magnetic energy $W_M$ (d)–(f). The number of the spectral components considered results adequate for all the viscosity profiles.

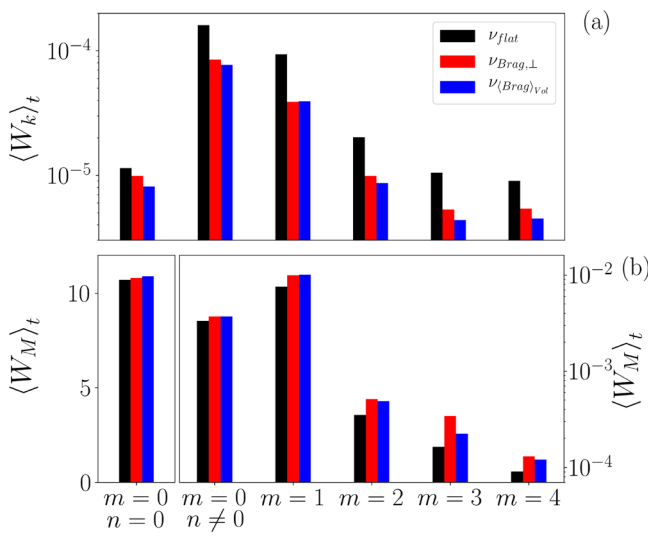


**FIG. 3.** Kinetic (a) and magnetic (b) energy spectrum comparison distinguishing the contribution of the axisymmetric component and of the MHD instabilities: The latter contributions are divided on the basis of the poloidal wave number. Note that panel (b) is divided into two subplots, with very different scales, one for the axisymmetric mode and another for the others. In both the cases: $\nu_{Brag,\perp}$ and $\nu_{\langle Brag\rangle_{Vol}}$, a reduction of the kinetic energy and an enhancement of the magnetic energy are observed for the fluctuating components.

effect (amounting to about a factor 0.5) of a higher viscosity profile on the kinetic energy is highlighted, in panels (a) and (b) for all the modes. In (d) and (e), the consequent enhancement (amounting to about a factor 1.3) of the magnetic field energy is shown. This is consistent with the expectation that the increased viscosity produces a stronger flow damping. In addition, the higher viscosity profile causes an increase in the magnetic activity.

The ratios shown in (c) and (f) are more interesting, because two viscosity profiles with the same volume average value are compared, being distinguished only by the "profile shape." In this case, the effect on the spectrum is smaller (amounting to about the 20% for both $W_k$, $W_M$), but anyway remarkable. In addition, the result of the comparison depends on the specific mode considered. Indeed, the kinetic energy of the $m = 1$ intermediate resonant modes is reduced, while that of the innermost resonant modes ($m = 1$, $n = -7, -8$) is increased by the $\nu_{Brag,\perp}$ profile. The opposite effect is observed for the magnetic energy. Despite a bulk viscosity increase in about a factor three causes a halving of the $m = 0$ kinetic energy, the influence of the profile in the behavior of the $m = 0$ is less clear. The latter may be influenced by the lower values of the plasma flow as the plasma edge is approached (see Fig. 8), which would make the damping viscosity effect less influential on the global plasma dynamics, since the velocity field is already weaken by the no-slip boundary conditions, see Sec. II.

Before analyzing the viscosity profile effects on the velocity and magnetic fields, we recall that a volume average viscosity larger by almost a factor three causes an increase in the energy associated with

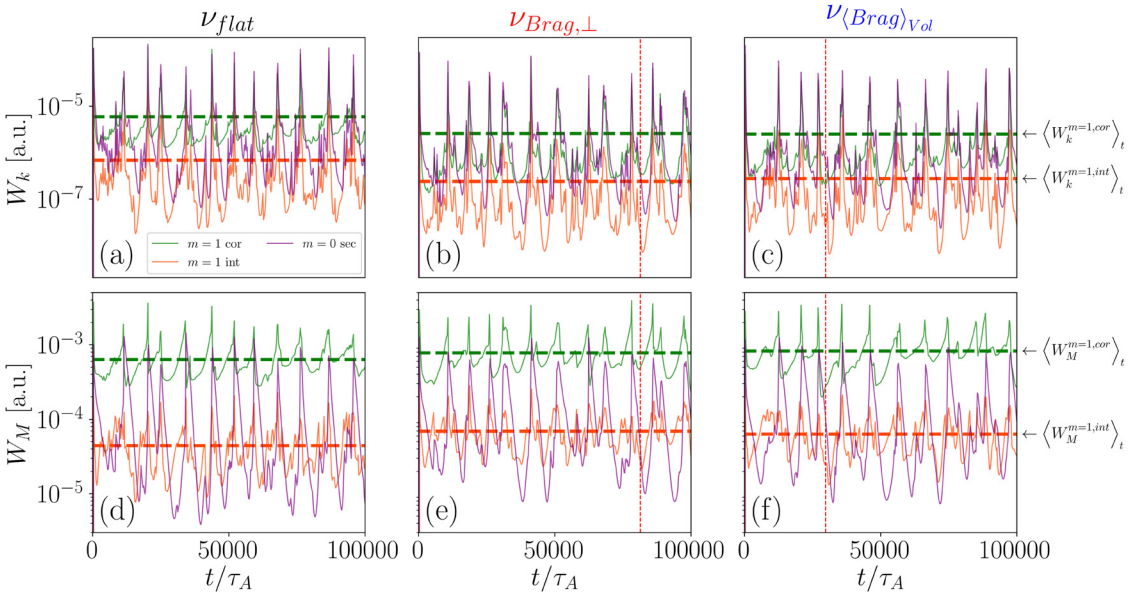


**FIG. 4.** Kinetic and magnetic energy time evolution comparison on the basis of the viscosity profile for $m=1$ and $m=0$ secondary modes, $-25 \le n \le -1$ (purple). The $m=1$ modes are grouped into two contributions: the $m=1$ core resonant modes, $-14 \le n \le -7$ (green), and the $m=1$ intermediate resonant modes, $-55 \le n \le -15$ (orange). The Braginskii-like viscosity profiles [(b), (c), (e), and (f)] display a reduction of the kinetic energy and a slight enhancement of the magnetic energy with respect to the flat profile [(a) and (d)]. This is pointed out by the dashed horizontal lines representing the time average of $m=1$ core resonant modes (green) and $m=1$ intermediate resonant modes (orange). The vertical lines indicate the time instants of the magnetic topology study, see Sec. VI: $t/\tau_A = 81\,360$ for $\nu_{\text{Brag},\perp}$ and $t/\tau_A = 29\,720$, for $\nu_{\langle\text{Brag}\rangle_{\text{Vol}}}$.

the magnetic fluctuations of ∼20%, see Fig. 3. In Fig. 7, the enhancement caused by the new viscosity profiles is shown in detail for the edge magnetic field fluctuations, splitting the contributions on the basis of the poloidal wave number.

In Fig. 8, the effect of the two profiles with equal volume average viscosity on the real field dynamics is analyzed. Being SpeCyl a spectral code, the real fields are computed by means of a Fourier anti-transform accounting for all the harmonics with poloidal mode numbers $m=0$, 1, and 2. Since the real field depends on position, the cylindrical surface average is computed at three selected radial positions: $r/a = 0.5, 0.7, 0.9$. The quantities considered for the comparison are the poloidal velocity $|v_\theta|$, the shear of the poloidal velocity $|sh(v_\theta)| = |dv_\theta/dr|$, and the unstable radial magnetic field $|b_r|$. We preliminary notice that the dynamics is not qualitatively altered by the new settings and that both the poloidal velocity and the radial magnetic field component are lowered as

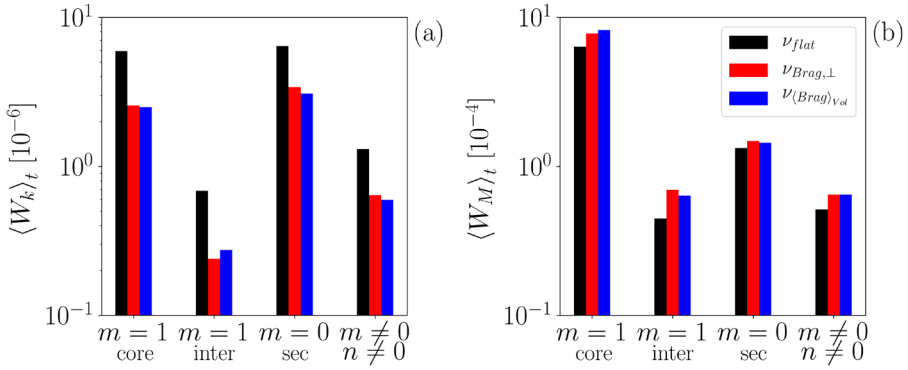


**FIG. 5.** Kinetic (a) and magnetic (b) energy time average comparison for the three different viscosity profiles. The average over four groups of modes are shown: the $m=1$ core and intermediate, the $m=0$ secondary, and the average of all the non-axisymmetric modes. The effects specifically due to the viscosity profile are pointed out. The $m=1$ core resonant modes resonate in the region where the Braginskii viscosity is lower than its volume average: their kinetic energy is enhanced, and their magnetic energy is dumped. On the other hand, the $m=1$ intermediate resonant modes resonate in a region where the Braginskii viscosity is larger than its volume average: their kinetic energy is damped and their magnetic energy is enhanced.

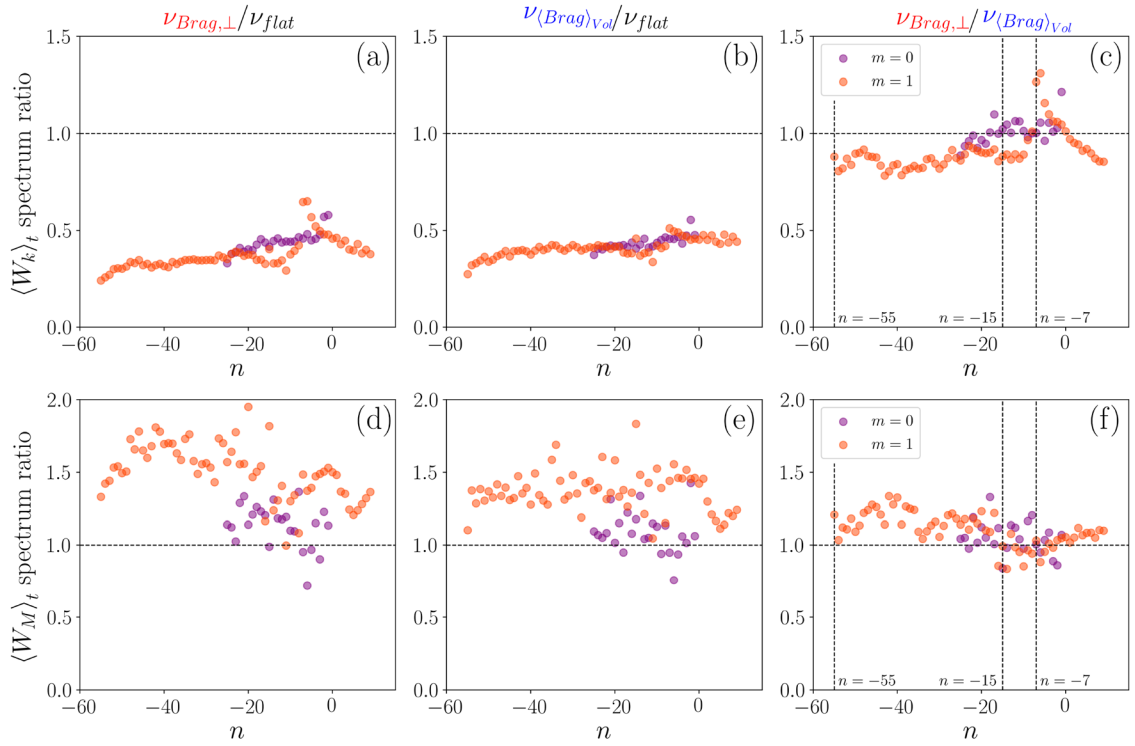


**FIG. 6.** Energy spectrum ratios for the $m=1$ and $m=0$ modes. Due to higher volume average viscosity $\nu_{\text{Brag},\perp}$ and $\nu_{\langle\text{Brag}\rangle_{\text{Vol}}}$, both cause a suppression of the kinetic energy (a) and (b), in correspondence of which an enhancement of the magnetic energy is observed (d) and (e). In (c) and (f), the pure effect of the profile is highlighted displaying, for the $m=1$ modes, a damp of the kinetic energy (and the associated grow of the magnetic energy) for the modes with $n \leq -15$ and the opposite effect for the core resonant modes.

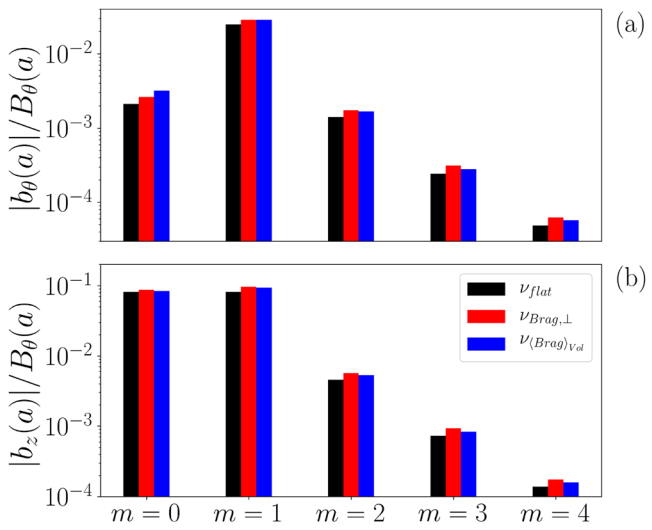


**FIG. 7.** Edge magnetic field instabilities, normalized to the edge poloidal magnetic field for the azimuthal (a) and axial (b) components. The Braginskii-like viscosity profiles ($\nu_{\text{Brag},\perp}$ and $\nu_{\langle\text{Brag}\rangle_{\text{Vol}}}$) enhance the magnetic fluctuation amplitudes.

the plasma edge is approached, according to the boundary conditions settings.

To evaluate the effects purely due to the viscosity profile, the time average ratio of the average fields is calculated and summarized in Table II. The latter is computed excluding the reconnection events, i.e., choosing the time intervals during which the spectral index[56] is below a fixed threshold: $N_s \leq 5$.

Though small, a decrease amounting to about the 20% of the absolute value is observed for the poloidal velocity, by taking a non-uniform $\nu$ profile. It is worth noting that the decrease affecting the shear of the poloidal velocity is even larger and it cannot be explained only in terms of velocity damping, but suggests a more direct (damping) effect of the viscosity profile on the shear of the velocity (as expected, since the stress tensor depends on the spatial derivatives of the velocity). On the contrary, the suppression effect on the shear flow has a small enhancing effect (∼5%) on the radial magnetic field. This result (derived in the contest of numerical macroscopic instability studies) recalls a well-known mechanism of microturbulence suppression induced by edge shear flow, analytically derived in Ref. 36 for the tokamak configuration. In that framework, an increase in the electric field (and of its shear), triggers, thanks to the interaction with the (mainly toroidal) magnetic field, the onset of a sheared poloidal rotation ($v_\theta = E_r \times B_\phi$), which is able to quench the magnetic turbulence.

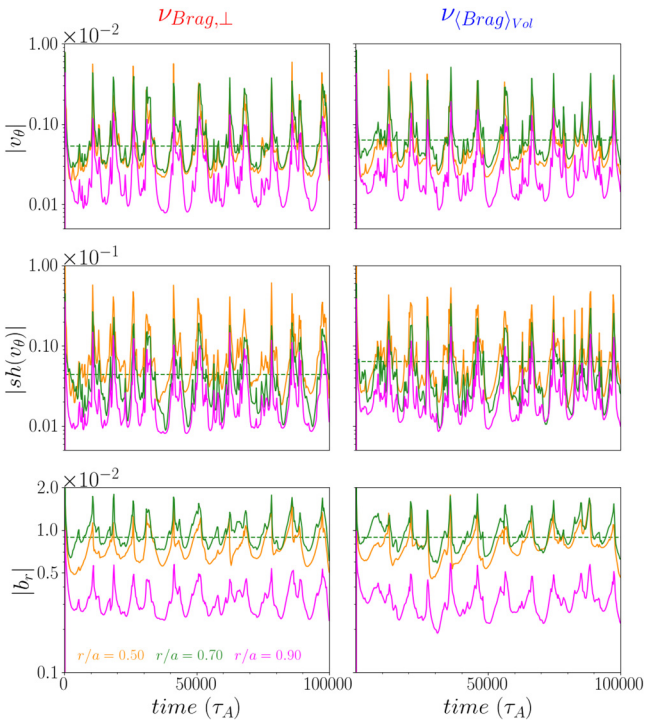


**FIG. 8.** Comparison of the poloidal velocity, shear of the poloidal velocity, and radial magnetic field evolution in time, displayed for the profiles $\nu_{\langle Brag\rangle_{Vol}}$ and $\nu_{Brag,\perp}$ to test the "pure" profiles effects. The average over the cylindrical surfaces at the radial positions $r/a = 0.5, 0.7, 0.9$ are considered and computed every $250\tau_A$. For the radial position $r/a = 0.70$, the time average of $v_\theta$, $sh(v_\theta)$ and $b_r$ is also computed and represented by the green horizontal dashed lines. Despite not qualitatively altering the dynamics, both the flow and the shear flow are damped by the $\nu_{Brag,\perp}$ profile.

Here, on the contrary, the decrease in macroscopic plasma flow has an enhancing effect on macroscopic magnetic instabilities.

## V. PROFILE EFFECTS ON THE VISCOSITY ANOMALY

In this section, the potential effect of adopting a Braginskii viscosity profile on the viscosity anomaly is discussed.

First of all, we recall that many studies in the past[22–26] have highlighted the existence of a viscosity anomaly (amounting to about two orders of magnitude) between experimental measurements and the Braginskii estimate of the perpendicular viscosity in RFP plasmas.

**TABLE II.** Time average of the poloidal velocity, shear velocity, and radial magnetic field at selected radial positions, calculated excluding the reconnection events. The values highlight a moderate damp of the poloidal flow and the shear poloidal flow: $v_\theta^{Brag,\perp}/v_\theta^{\langle Brag\rangle_{Vol}} \leq 1$ and $v_\theta^{Brag,\perp}/v_\theta^{\langle Brag\rangle_{Vol}} \leq 1$ and a moderate enhancement of the magnetic field $b_r^{Brag,\perp}/b_r^{\langle Brag\rangle_{Vol}} \geq 1$.

| | $v_\theta^{Brag,\perp}/v_\theta^{\langle Brag\rangle_{Vol}}$ | $sh_\theta^{Brag,\perp}/sh_\theta^{\langle Brag\rangle_{Vol}}$ | $b_r^{Brag,\perp}/b_r^{\langle Brag\rangle_{Vol}}$ |
|---|---|---|---|
| $r/a = 0.50$ | 1.02 | 0.84 | 1.07 |
| $r/a = 0.70$ | 0.81 | 0.69 | 1.02 |
| $r/a = 0.90$ | 0.91 | 0.83 | 0.95 |

The measurements are based on the study of plasma flow damping, consequent to momentum injection by means of a probe (biased electrode) or resonant magnetic perturbations (RMP). The existence of a viscosity anomaly is also found comparing the fitting laws of the $m = 1$ secondary modes amplitude (i.e., $-20 \leq n \leq -8$) of the magnetic field as a function of Hartmann number, for SpeCyl numerical simulations and RFX-mod experimental data, which is shown in Fig. 6 of Ref. 52.

The two scaling laws are both calculated with an ordinary least squares technique on a wide database of SpeCyl simulations exploiting a flat viscosity profile[10] and RFX-mod experimental data.[57] The on-axis value of the Hartmann number is considered as an independent variable of the scaling, since this is the only estimate of the dimensionless number available in the experimental data. In that case, we noticed that the simulations and the experimental data display a similar trend of decreasing amplitudes with increasing Hartmann, if the latter is evaluated (for the experimental data) according to the perpendicular Braginskii viscosity. However, an important anomaly was highlighted: $H_{SpeCyl}/H_{exp} \sim 0.07$. The difference between the two set of data can be solved by rescaling the Hartmann number. Thus, the origin of the anomaly can be attributed to an anomaly of either plasma resistivity or viscosity with respect to the Braginskii formulation. If one attributes the anomaly to the viscosity only, one gets a $\delta := \nu_{exp}/\nu_{Brag,\perp} \sim 250$ anomaly factor.

We observe in this study that the introduction of a perpendicular Braginskii profile $\nu_{Brag,\perp}$ of the viscosity (maintaining the same on-axis viscosity value $\nu_0$, for the consistency with the experimental data) causes an increase in the $m = 1$ secondary modes of about 13%. This can contribute, albeit not decisively, to reducing the offset of about a factor 3, bringing its value to $\delta \sim 75$–$100$. Even if not sufficient to explain the viscosity anomaly on its own, the introduction of a Braginskii-like viscosity profile is potentially relevant for future improvements of the viscosity estimate.

## VI. BRAGINSKII-LIKE VISCOSITY PROFILE: MAGNETIC TOPOLOGY EFFECTS

In this section, we test the effect of the change of viscosity profile on the magnetic field lines topology. To do so, two tools are employed, namely, the Poincaré plot and the connection length (CL).

The Poincaré plot is a well known method to study recurrent flows in a dynamical system. It is based on the definition of puncture plot of a vector field (in this case the magnetic field) on a so-called Poincaré section $\mathcal{S}$. The puncture plot is the intersection of a magnetic field line with $\mathcal{S}$, indicated by $p_i \in \mathcal{S}$ with $i$ indicating the ordering of the intersections. The Poincaré plot is the union of all puncture plots. (Of course, in the pictures, we plot a finite set of puncture plots.)

The connection length represents the arc length that a magnetic field line threads from an initial condition to reach a selected radial position (usually the wall) $r_{thr}$. It is defined as the average between the length to reach $r_{thr}$ following the magnetic field forward and backward.

As a preliminary test of the effect of the radial dependence of the viscosity profile on magnetic topology, we select two time snapshots from the two simulations: one with the perpendicular Braginskii viscosity profile and the other one with the flat profile.

The two snapshots are chosen by looking for a similar dynamical phase and to reflect the differences in the magnetic spectrum during the whole simulation shown in Fig. 6(f), i.e., similar magnetic energy

associated with the $m=1$ core resonant modes ($-15 < n < -7$) and a higher value of magnetic energy associated with the $m=1$ intermediate resonant modes ($-55 \leq n \leq -15$).

This is respected by the two snapshots, and, keeping in mind that a single time snapshot may be partially representative of the whole simulation, the impact will emerge in the topological properties, as we will show.

The two snapshots are selected: at $t = 81\,360\tau_A$, in the simulation with the perpendicular Braginskii viscosity profile $\nu_{Brag,\perp}$ and at $t = 29\,720\tau_A$, in the one with volume averaged profile equal to the Braginskii one $\nu_{\langle Brag\rangle_{Vol}}$. In Fig. 4, the two snapshots are highlighted with a dashed line in the subplots (b) and (e) and (c) and (f).

### 1. Poincaré plot analysis

In Fig. 9, two sets of Poincaré plots are presented. The results about the simulation with a Braginskii viscosity profile $\nu_{Brag,\perp}$ are depicted in panels (a) and (c).

Panel (a) presents a Poincaré plot on a surface $\mathscr{S}$ at a fixed poloidal angle $\theta_{\mathscr{S}} = 0$: This surface of section highlights the periodicity of the magnetic field structures along the $z$ direction. One can observe a tiny structure with a periodicity $n=7$ at $r \sim 0.15a$ and a more evident structure of islands at $r \sim 0.8a$. Panel (c) is a Poincaré plot on a surface at a fixed axial position $z_{\mathscr{S}} = 0$: This surface of section shows that the chain of islands at $r \sim 0.8a$ has a "poloidally symmetric" (i.e., $m=0$) structure. It is also visible that the structures in the core have an $m=1$ periodicity: In fact, the region $r \sim 0.15a$ is the one, where the $m=1, n=-7$ MHD mode is more active and the related eigenfunction has a higher value than all the other ones. Such a value is higher enough than all the other MHD modes to allow for the emergence of a small conserved structure in that region.

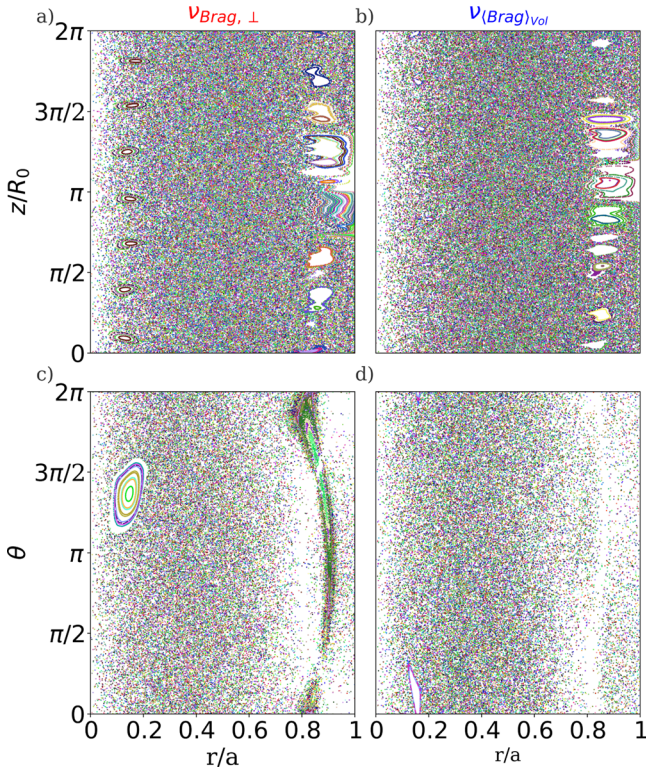


**FIG. 9.** Poincaré plots comparison for SpeCyl simulations with different viscosity profiles for selected time instants: $t/\tau_A = 81\,360$ for $\nu_{Brag,\perp}$ in panels (a) and (c) and $t/\tau_A = 29\,720$ for $\nu_{\langle Brag\rangle_{Vol}}$ in panels (b) and (d). Poincaré sections $\mathscr{S}$ are taken at $\theta = 0$ [panels (a) and (b)] and $z = 0$ [panels (c) and (d)]. Wider structures are observed in the core in both panels (a) and (c). This is due to the fact that the marginally resonant $m=1, n=-7$ MHD mode presents an eigenfunction quite peaked in the region $r/a \sim 0.10$ in the $\nu_{Brag,\perp}$ simulation. On average, the energy associated with the intermediate resonant $m=1$ modes is higher than the simulation with the flat viscosity profile, in agreement with the analysis presented in Sec. IV.

Panels (b) and (d) describe the magnetic topology of the simulation with the $\nu_{\langle Brag\rangle_{Vol}}$ flat viscosity profile. For the two instants chosen, the viscosity profile does not alter qualitatively the Poincaré plots, which appear to be similar. Indeed, only a careful analysis reveals the existence of small quantitative differences. In particular, one notices in panels (b) and (d) smaller conserved structures with $n=7$ periodicity, close to the core (corresponding to a $m=1$, $n=-7$ mode dominant in this region). Instead, the ones with $m=0$ close to the edge cover a slightly larger area than the corresponding ones in panels (a) and (c). A possible explanation of this behavior lies in the fact that in the $\nu_{Brag,\perp}$ simulation, the MHD modes more active in the core have an increased amplitude, as described in Sec. IV and at the beginning of this section.

### 2. Connection length analysis

To make the previous consideration more quantitative, we show the connection length in Fig. 10, computed on the $\theta_{\mathscr{S}} = 0$ surface of section.

Panel (a) regards the simulation with $\nu_{Brag,\perp}$, while panel (b) regards the simulation with $\nu_{\langle Brag\rangle_{Vol}}$. Both panels show the CL to the edge ($r_{thr} = a$) of magnetic field lines starting on the $\theta_{\mathscr{S}} = 0$ surface.

Consider panel (a). One notices a much higher connection length (very close to the maximum value over which the computation is

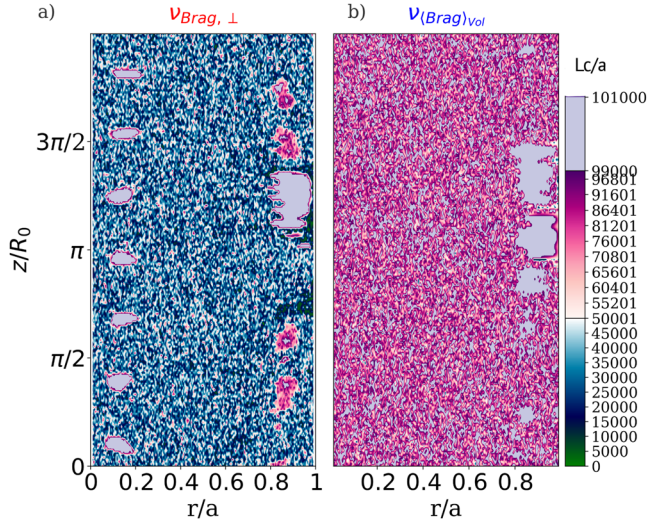


**FIG. 10.** Plots of the connection length comparison for SpeCyl simulations for $\nu_{Brag,\perp}$ in panel (a) and $\nu_{\langle Brag\rangle_{Vol}}$ in panel (b). The time snapshots and sections coincide with those of Fig. 9.

stopped by the field line tracing code, in this case $L_{c,\max} = 10^5$ in normalized units) in the region where conserved magnetic surfaces are present, both in the core and at the edge. One can observe that the chain of $m = 0$ magnetic islands at the edge, observed in Figs. 9(a) and 9(b), represents a partial barrier,[46] preventing the escape of some magnetic field lines. Also, it is interesting to notice the presence of an edge region, at $z/R_0 \sim 3\pi/4$, with very low connection length. This is probably the region where high-n modes lock with each other, see Ref. 58.

Panel (b), similarly, regards the simulation with $\nu_{\langle Brag \rangle_{Vol}}$. One notices that the average connection length is higher than that in the simulation with a Braginskii profile [panel (a)]. A simple average of the CL at $z = 0$ provides, in fact, a value of $\langle L_c \rangle^{Brag_\perp} \sim 4 \times 10^4$ on the left and $\langle L_c \rangle^{\langle Brag \rangle_{Vol}} \sim 8 \times 10^4$ on the right, a remarkable difference, more evident than that displayed by the Poincaré plots. For both viscosity profiles, one finds the edge region with extremely low connection length: In panel (b), it is observed at $z \sim \pi R_0$.

A reasonable interpretation is that the higher magnetic activity in the simulation with a non-flat viscosity profile results in a negative effect on the overall transport of magnetic field lines, visible through the lower average CL in panel (a): In fact, higher MHD modes imply a higher stochasticity of the magnetic field lines and a higher transport of magnetic field lines and thus a lower connection length.

## VII. CONCLUSIONS AND FINAL REMARKS

In this paper, we have presented a sensitivity study of the Braginskii experimental-like profile effects on non-linear visco-resistive MHD simulations.

The effects of three different viscosity profiles have been compared, allowing us to highlight the existence of local effects specifically due to the profile, in addition to the more consistent ones, due to the absolute value of the viscosity. The latter have already been highlighted in the past (see, e.g., Ref. 10), jointly varying resistivity and viscosity. The present work is consistent with that study, if the same Hartmann regime ($H \sim 10^5$) is considered.

The effects have been studied considering plasma dynamics and magnetic field topology. About the simulation dynamics, the profile effect has consisted of a: kinetic energy, velocity field, and shear velocity (small) damping and in a correspondent enhancement of the magnetic field and the magnetic energy. This is specifically highlighted in the case of $m = 1$ intermediate resonant modes ($n \leq -15$), which resonates in regions, where the Braginskii viscosity profile is larger. About the magnetic topology, the Poincaré plots and the connection length contour-plot have been shown at specific time instants (far from the reconnection events), displaying larger structures with conserved magnetic surfaces for the perpendicular Braginskii profile, sign of a more intense MHD activity, due to the $m = 1$ intermediate resonant modes. In turns, this results in an increased level of transport of magnetic field lines, as shown by the connection length plots, in Fig. 10.

The new profiles have also been proved to provide a slight reduction of the anomaly in viscosity[21–26] observed between the simulation and experimental data. Indeed, the introduction of a Braginskii-like viscosity profile in SpeCyl numerical simulations would slightly contribute to decreasing the offset displayed when comparing the scaling laws of $m = 1$ magnetic field edge instabilities as a function of the Hartmann number for SpeCyl numerical simulations and RFX-mod experimental data.[52]

Some assumptions made in the simulations presented in this work deserve additional remarks. In particular, we point out that the approximation of constant, uniform density (made in SpeCyl) corresponds to the experimental observation and it strictly holds only if the density profile evolution can be considered slow with respect to that of velocity and magnetic field profiles.[37] In this case, to formally satisfy the continuity equation (not evolved in SpeCyl), artificial "source/sink" terms should be assumed as a simplified representation of the time-dependent inflows/outflows from the plasma wall. (A refined plasma–wall interaction modeling is indeed largely beyond the scope of this work.) A more refined approximation for the density (polynomial function) is adopted in the estimate of the Braginskii like viscosity profile. The corresponding non-uniform density profile is not implemented in the simulations, to keep the same conditions (other than the viscosity profile) for the distinct simulations, thus estimating the pure effect of viscosity profile. Regarding the choice of the Bessel function model for the magnetic field, we remark that the difference introduced by using the latter instead of the code output is small, if compared to the uncertainty associated with the choice of an optimal formula to estimate the viscosity or to the assumptions of the simple visco-resistive model. The magnetic field output is going to be considered in the future, to upgrade this work with the introduction of a self-consistent viscosity evolution, despite being a task beyond the scope of the present study. Future developments could be considered for this work, addressing the effects of the additional terms introduced in momentum balance equation by a non-uniform viscosity profile, reported in App. A and the (already mentioned) introduction of a self-consistent evolution for the transport coefficients. We remark that the latter would require to solve a more complete set of MHD equations (including continuity and energy balance equations in the MHD model), because of the transport coefficients dependence on density and temperature. Since the more complete set of equations is not solved in SpeCyl, the use of a more complete MHD code, see, e.g., Ref. 31, has to be considered to get the time evolution of temperature and density and a self-consistent treatment of the transport coefficients. This further step in modeling, which is meant as long term development, would allow the resistivity and the viscosity to depend on all the spatial coordinates, testing whether this could have a positive feedback effect on the RFP helical self-organization process.

## ACKNOWLEDGMENTS

The authors would like to thank P. Zanca for carefully reading the manuscript and D.F. Escande for helpful interactions and useful suggestions. The authors acknowledge the use of the computational resources provided by the EUROfusion High Performance Computer (Marconi-Fusion) through the EUROfusion project named "PIXIE3D," which includes the topological studies described in Sec. VI.

This work has been carried out within the framework of the EUROfusion Consortium, funded by the European Union via the Euratom Research and Training Programme (Grant Agreement No. 101052200—EUROfusion). Views and opinions expressed are, however, those of the authors only and do not necessarily reflect those of the European Union or the European Commission. Neither the European Union nor the European Commission can be held responsible for them.

## AUTHOR DECLARATIONS

### Conflict of Interest

The authors have no conflicts to disclose.

### Author Contributions

**Nicholas Vivenzi:** Data curation (equal); Investigation (equal); Visualization (equal); Writing – original draft (equal). **Marco Veranda:** Data curation (equal); Formal analysis (equal); Supervision (equal); Writing – review & editing (equal). **Daniele Bonfiglio:** Supervision (equal); Writing – review & editing (equal). **Susanna Cappello:** Supervision (equal); Writing – review & editing (equal).

## DATA AVAILABILITY

The data that support the findings of this study are available from the corresponding author upon reasonable request.

## APPENDIX: MOMENTUM BALANCE EQUATION WITH A NON-UNIFORM VISCOSITY PROFILE

In this section, we report the modifications to the momentum balance equation introduced by considering a non-uniform viscosity profile. Since this work is intended to be a first order sensitivity study, these computations have not been taken into account in the present work, but they could be of interest for future developments. The viscosity term appears in the momentum balance equation as a tensor $\mathbf{\Pi}$, signal of the non-isotropic nature of transport in fusion plasmas. The tensor $\mathbf{\Pi}$ is usually simplified, assuming the proportionality to a rate-of-strain tensor as in neutral fluids,

$$\rho_0\left(\frac{\partial \mathbf{v}}{\partial t}+(\mathbf{v}\cdot\nabla)\mathbf{v}\right)=-\nabla p+\mathbf{j}\times\mathbf{B}-\nabla\cdot\mathbf{\Pi}, \tag{A1}$$

$$\mathbf{\Pi}=-\mu\mathbf{W}, \tag{A2}$$

$$\mathbf{\Pi}_{ij}=-\mu\left(\frac{\partial v_i}{\partial x_j}+\frac{\partial v_j}{\partial x_i}-\frac{2}{3}(\nabla\cdot\mathbf{v})\delta_{ij}\right), \tag{A3}$$

where $\mu$ represents the dynamic viscosity, which differs with respect to the kinematic viscosity $\nu$ (used in the rest of the paper) by the mass density factor $\rho_0$, assumed to be uniform and constant in SpeCyl, $\mu := \rho_0\nu$. Expliciting the indices for a non-uniform $\mu(\mathbf{r})$, one gets

$$\begin{aligned}-(\nabla\cdot\mathbf{\Pi})_i=\sum_j\frac{\partial\mathbf{\Pi}_{ij}}{\partial x_j}&=\sum_j\frac{\partial}{\partial x_j}\left[\mu\left(\frac{\partial v_i}{\partial x_j}+\frac{\partial v_j}{\partial x_i}-\frac{2}{3}(\nabla\cdot\mathbf{v})\delta_{ij}\right)\right]\\&=\sum_j\frac{\partial\mu}{\partial x_j}\left(\frac{\partial v_i}{\partial x_j}+\frac{\partial v_j}{\partial x_i}-\frac{2}{3}(\nabla\cdot\mathbf{v})\delta_{ij}\right)\\&\quad+\sum_j\mu\left(\frac{\partial^2 v_i}{\partial x_j^2}+\frac{\partial^2 v_j}{\partial x_j\partial x_i}\right)-\frac{2}{3}\frac{\partial}{\partial x_i}(\nabla\cdot\mathbf{v})\\&=\sum_j\left(\frac{\partial\mu}{\partial x_j}\frac{\partial v_i}{\partial x_j}+\frac{\partial\mu}{\partial x_j}\frac{\partial v_j}{\partial x_i}\right)-\frac{2}{3}\frac{\partial\mu}{\partial x_i}(\nabla\cdot\mathbf{v})\\&\quad+\mu\nabla^2 v_i+\frac{1}{3}\mu\frac{\partial}{\partial x_i}(\nabla\cdot\mathbf{v}).\end{aligned} \tag{A4}$$

The momentum balance equation is so rewritten as

$$\begin{aligned}\rho_0\left(\frac{\partial\mathbf{v}}{\partial t}+(\mathbf{v}\cdot\nabla)\mathbf{v}\right)&=-\nabla p+\mathbf{j}\times\mathbf{B}+(\nabla\mu\cdot\nabla)\mathbf{v}\\&\quad+\nabla\mu:\nabla\mathbf{v}-\frac{2}{3}(\nabla\cdot\mathbf{v})\nabla\mu\\&\quad+\mu\nabla^2\mathbf{v}+\frac{1}{3}\mu\nabla(\nabla\cdot\mathbf{v}).\end{aligned} \tag{A5}$$

In addition to the diffusive term $\mu\nabla^2\mathbf{v}$, other terms should be considered. Two of them are proportional to $\nabla\cdot\mathbf{v}$ and could be neglected if the hypothesis of uncompressible fluid is made. The other terms should be computed using the specific spatial dependence of the profile.

## REFERENCES


[1] J. Freidberg, *Ideal MHD* (Cambridge University Press, 2014).
[2] L. Marrelli, P. Martin, M. E. Puiatti, J. S. Sarff, B. E. Chapman, J. R. Drake, D. F. Escande, and S. Masamune, "The reversed field pinch," Nucl. Fusion **61**, 023001 (2021).
[3] R. Lorenzini, E. Martines, P. Piovesan, D. Terranova, P. Zanca, M. Zuin, A. Alfier, D. Bonfiglio, F. Bonomo, A. Canton, S. Cappello, L. Carraro, R. Cavazzana, D. F. Escande, A. Fassina, P. Franz, M. Gobbin, P. Innocente, L. Marrelli, R. Pasqualotto, M. E. Puiatti, M. Spolaore, M. Valisa, N. Vianello, P. Martin, and RFX-mod team and collaborators, "Self-organized helical equilibria as a new paradigm for ohmically heated fusion plasmas," Nat. Phys. **5**, 570–574 (2009).
[4] S. Cappello and R. Paccagnella, "Nonlinear plasma evolution and sustainment in the reversed field pinch," Phys. Fluids B **4**, 611–618 (1992).
[5] J. M. Finn, R. Nebel, and C. Bathke, "Single and multiple helicity ohmic states in reversed-field pinches," Phys. Fluids B **4**, 1262–1279 (1992).
[6] P. Piovesan, M. Zuin, A. Alfier, D. Bonfiglio, F. Bonomo, A. Canton, S. Cappello, L. Carraro, R. Cavazzana, D. F. Escande, A. Fassina, M. Gobbin, R. Lorenzini, L. Marrelli, P. Martin, E. Martines, R. Pasqualotto, M. E. Puiatti, M. Spolaore, M. Valisa, N. Vianello, P. Zanca, and the RFX-mod Team, "Magnetic order and confinement improvement in high-current regimes of RFX-mod with MHD feedback control," Nucl. Fusion **49**, 085036 (2009).
[7] J. Sarff, A. Almagri, J. Anderson, M. Borchardt, D. Carmody, K. Caspary, B. Chapman, D. D. Hartog, J. Duff, S. Eilerman, A. Falkowski, C. Forest, J. Goetz, D. Holly, J.-H. Kim, J. King, J. Ko, J. Koliner, S. Kumar, J. Lee, D. Liu, R. Magee, K. McCollam, M. McGarry, V. Mirnov, M. Nornberg, P. Nonn, S. Oliva, E. Parke, J. Reusch, J. Sauppe, A. Seltzman, C. Sovinec, H. Stephens, D. Stone, D. Theucks, M. Thomas, J. Triana, P. Terry, J. Waksman, W. Bergerson, D. Brower, W. Ding, L. Lin, D. Demers, P. Fimognari, J. Titus, F. Auriemma, S. Cappello, P. Franz, P. Innocente, R. Lorenzini, E. Martines, B. Momo, P. Piovesan, M. Puiatti, M. Spolaore, D. Terranova, P. Zanca, V. Belykh, V. Davydenko, P. Deichuli, A. Ivanov, S. Polosatkin, N. Stupishin, D. Spong, D. Craig, R. Harvey, M. Cianciosa, and J. Hanson, "Overview of results from the MST reversed field pinch experiment," Nucl. Fusion **53**, 104017 (2013).
[8] D. F. Escande, R. Paccagnella, S. Cappello, C. Marchetto, and F. D'Angelo, "Chaos healing by separatrix disappearance and quasisingle helicity states of the reversed field pinch," Phys. Rev. Lett. **85**, 3169–3172 (2000).
[9] D. Bonfiglio, M. Veranda, S. Cappello, D. F. Escande, and L. Chacón, "Experimental-like helical self-organization in reversed-field pinch modeling," Phys. Rev. Lett. **111**, 085002 (2013).
[10] M. Veranda, D. Bonfiglio, S. Cappello, G. di Giannatale, and D. F. Escande, "Helically self-organized pinches: Dynamical regimes and magnetic chaos healing," Nucl. Fusion **60**, 016007 (2019).
[11] J. W. Bates and D. C. Montgomery, "Toroidal visco-resistive magnetohydrodynamic steady states contain vortices," Phys. Plasmas **5**, 2649–2653 (1998).
[12] L. P. J. Kamp and D. C. Montgomery, "Toroidal steady states in visco-resistive magnetohydrodynamics," J. Plasma Phys. **70**, 113–142 (2004).
[13] X. Shan and D. Montgomery, "Global searches of Hartmann-number-dependent stability boundaries," Plasma Phys. Controlled Fusion **35**, 1019 (1993).

[14]D. Montgomery and X. Shan, "Toroidal resistive MHD equilibria," Comments Plasma Phys. Controlled Fusion **15**, 315–320 (1994).
[15]J. A. Morales, W. J. T. Bos, K. Schneider, and D. C. Montgomery, "The effect of toroidicity on reversed field pinch dynamics," Plasma Phys. Controlled Fusion **56**, 095024 (2014).
[16]S. Cappello and D. F. Escande, "Bifurcation in viscoresistive MHD: The Hartmann number and the reversed field pinch," Phys. Rev. Lett. **85**, 3838–3841 (2000).
[17]M. R. Stoneking, J. T. Chapman, D. J. Den Hartog, S. C. Prager, and J. S. Sarff, "Experimental scaling of fluctuations and confinement with Lundquist number in the reversed-field pinch," Phys. Plasmas **5**, 1004–1014 (1998).
[18]S. I. Braginskii, *Reviews of Plasma Physics* (Consultants Bureau, New York, 1965), Vol. 1, pp. 205–311.
[19]K. F. Schoenberg, R. W. Moses, Jr., and R. L. Hagenson, "Plasma resistivity in the presence of a reversed-field pinch dynamo," Phys. Fluids **27**, 1671–1676 (1984).
[20]E. A. Saad and P. R. Brunsell, "Experimental characterization and modelling of the resistive wall mode response in a reversed field pinch," Plasma Phys. Controlled Fusion **64**, 055011 (2022).
[21]J. M. Finn, P. N. Guzdar, and A. A. Chernikov, "Particle transport and rotation damping due to stochastic magnetic field lines," Phys. Fluids B **4**, 1152–1155 (1992).
[22]A. F. Almagri, J. T. Chapman, C. S. Chiang, D. Craig, D. J. Den Hartog, C. C. Hegna, and S. C. Prager, "Momentum transport and flow damping in the reversed-field pinch plasma," Phys. Plasmas **5**, 3982–3985 (1998).
[23]B. E. Chapman, R. Fitzpatrick, D. Craig, P. Martin, and G. Spizzo, "Observation of tearing mode deceleration and locking due to eddy currents induced in a conducting shell," Phys. Plasmas **11**, 2156–2171 (2004).
[24]L. Frassinetti, S. Menmuir, K. E. J. Olofsson, P. R. Brunsell, and J. R. Drake, "Tearing mode velocity braking due to resonant magnetic perturbations," Nucl. Fusion **52**, 103014 (2012).
[25]R. Fridström, B. E. Chapman, A. F. Almagri, L. Frassinetti, P. R. Brunsell, T. Nishizawa, and J. S. Sarff, "Dependence of perpendicular viscosity on magnetic fluctuations in a stochastic topology," Phys. Rev. Lett. **120**, 225002 (2018).
[26]D. Craig, E. H. Tan, B. Schott, J. K. Anderson, J. Boguski, D. J. Den Hartog, T. Nishizawa, M. D. Nornberg, and Z. A. Xing, "Intrinsic flow and tearing mode rotation in the RFP during improved confinement," Phys. Plasmas **26**, 072503 (2019).
[27]F. Trintchouk, M. Yamada, H. Ji, R. M. Kulsrud, and T. A. Carter, "Measurement of the transverse Spitzer resistivity during collisional magnetic reconnection," Phys. Plasmas **10**, 319–322 (2003).
[28]A. Kuritsyn, M. Yamada, S. Gerhardt, H. Ji, R. Kulsrud, and Y. Ren, "Measurements of the parallel and transverse Spitzer resistivities during collisional magnetic reconnection," Phys. Plasmas **13**, 055703 (2006).
[29]D. Montgomery, "Magnetohydrodynamic stability thresholds as a function of Hartmann number and pinch ratio," Plasma Phys. Controlled Fusion **34**, 1157–1162 (1992).
[30]W. Park, E. V. Belova, G. Y. Fu, X. Z. Tang, H. R. Strauss, and L. E. Sugiyama, "Plasma simulation studies using multilevel physics models," Phys. Plasmas **6**, 1796–1803 (1999).
[31]L. Chacón, "An optimal, parallel, fully implicit Newton-Krylov solver for three-dimensional viscoresistive magnetohydrodynamics," Phys. Plasmas **15**, 056103 (2008).
[32]M. Hoelzl, G. Huijsmans, S. Pamela, M. Becoulet, E. Nardon, F. J. Artola, B. Nkonga, C. Atanasiu, V. Bandaru, A. Bhole, D. Bonfiglio, A. Cathey, O. Czarny, A. Dvornova, T. Feher, A. Fil, E. Franck, S. Futatani, M. Gruca, H. Guillard, J. W. Haverkort, I. Holod, D. Hu, S. Kim, S. Q. Korving, L. Kos, I. Krebs, L. Kripner, G. Latu, F. Liu, P. Merkel, D. Meshcheriakov, V. Mitterauer, S. Mochalskyy, J. Morales, R. Nies, N. Nikulsin, F. Orain, D. Penko, J. Pratt, R. Ramasamy, P. Ramet, C. Reux, K. Särkimäki, N. Schwarz, P. S. Verma, S. F. Smith, C. Sommariva, E. Strumberger, D. van Vugt, M. Verbeek, E. Westerhof, F. Wieschollek, and J. Zielinski, "The JOREK non-linear extended MHD code and applications to large-scale instabilities and their control in magnetically confined fusion plasmas," Nucl. Fusion **61**, 065001 (2021).
[33]S. Cappello and D. Biskamp, "Reconnection processes and scaling laws in reversed field pinch magnetohydrodynamics," Nucl. Fusion **36**, 571 (1996).
[34]S. Futatani, J. A. Morales, and W. J. T. Bos, "Dynamic equilibria and magneto-hydrodynamic instabilities in toroidal plasmas with non-uniform transport coefficients," Phys. Plasmas **22**, 052503 (2015).
[35]A. M. Futch, D. Craig, R. Hesse, and C. M. Jacobson, "Role of resistivity and viscosity in the excitation of stable m = 0 modes during the RFP sawtooth crash," Phys. Plasmas **25**, 112506 (2018).
[36]H. Biglari, P. H. Diamond, and P. W. Terry, "Influence of sheared poloidal rotation on edge turbulence," Phys. Fluids B **2**, 1–4 (1990).
[37]D. Biskamp, *Nonlinear Magnetohydrodynamics, Cambridge Monographs on Plasma Physics* (Cambridge University Press, 1993).
[38]M. Veranda, D. Bonfiglio, S. Cappello, D. F. Escande, F. Auriemma, D. Borgogno, L. Chacón, A. Fassina, P. Franz, M. Gobbin, D. Grasso, and M. E. Puiatti, "Magnetohydrodynamics modelling successfully predicts new helical states in reversed-field pinch fusion plasmas," Nucl. Fusion **57**, 116029 (2017).
[39]H. R. Strauss, "The dynamo effect in fusion plasmas," Phys. Fluids **28**, 2786–2792 (1985).
[40]J. A. Holmes, B. A. Carreras, P. H. Diamond, and V. E. Lynch, "Nonlinear dynamics of tearing modes in the reversed field pinch," Phys. Fluids **31**, 1166–1179 (1988).
[41]K. Kusano and T. Sato, "Simulation study of the self-sustainment mechanism in the reversed field pinch configuration," Nucl. Fusion **30**, 2075 (1990).
[42]Y. L. Ho and G. G. Craddock, "Nonlinear dynamics of field maintenance and quasiperiodic relaxation in reversed-field pinches," Phys. Fluids B **3**, 721–734 (1991).
[43]C. R. Sovinec, J. M. Finn, and D. del Castillo-Negrete, "Formation and sustainment of electrostatically driven spheromaks in the resistive magnetohydrodynamic model," Phys. Plasmas **8**, 475–490 (2001).
[44]M. Puiatti, S. Cappello, R. Lorenzini, S. Martini, S. Ortolani, R. Paccagnella, F. Sattin, D. Terranova, T. Bolzonella, A. Buffa, A. Canton, L. Carraro, D. Escande, L. Garzotti, P. Innocente, L. Marrelli, E. Martines, P. Scarin, G. Spizzo, M. Valisa, P. Zanca, V. Antoni, L. Apolloni, M. Bagatin, W. Baker, O. Barana, D. Bettella, P. Bettini, R. Cavazzana, M. Cavinato, G. Chitarin, A. Cravotta, F. D'Angelo, S. D. Bello, A. D. Lorenzi, D. Desideri, P. Fiorentin, P. Franz, L. Frassinetti, E. Gaio, L. Giudicotti, F. Gnesotto, L. Grando, S. Guo, A. Luchetta, G. Malesani, G. Manduchi, G. Marchiori, D. Marcuzzi, P. Martin, A. Masiello, F. Milani, M. Moresco, A. Murari, P. Nielsen, R. Pasqualotto, B. Pégourie, S. Peruzzo, R. Piovan, P. Piovesan, N. Pomaro, G. Preti, G. Regnoli, G. Rostagni, G. Serianni, P. Sonato, E. Spada, M. Spolaore, C. Taliercio, G. Telesca, V. Toigo, N. Vianello, P. Zaccaria, B. Zaniol, L. Zanotto, E. Zilli, G. Zollino, and M. Zuin, "Analysis and modelling of the magnetic and plasma profiles during PPCD experiments in RFX," Nucl. Fusion **43**, 1057 (2003).
[45]P. Piovesan, D. Craig, L. Marrelli, S. Cappello, and P. Martin, "Measurements of the MHD dynamo in the quasi-single-helicity reversed-field pinch," Phys. Rev. Lett. **93**, 235001 (2004).
[46]G. Spizzo, S. Cappello, A. Cravotta, D. F. Escande, I. Predebon, L. Marrelli, P. Martin, and R. B. White, "Transport barrier inside the reversal surface in the chaotic regime of the reversed-field pinch," Phys. Rev. Lett. **96**, 025001 (2006).
[47]F. Ebrahimi, V. V. Mirnov, and S. C. Prager, "Momentum transport from tearing modes with shear flow," Phys. Plasmas **15**, 055701 (2008).
[48]R. Chahine and W. J. T. Bos, "On the role and value of $\beta$ in incompressible MHD simulations," Phys. Plasmas **25**, 042115 (2018).
[49]D. Bonfiglio, L. Chacón, and S. Cappello, "Nonlinear three-dimensional verification of the SPECYL and PIXIE3D magnetohydrodynamics codes for fusion plasmas," Phys. Plasmas **17**, 082501 (2010).
[50]S. Cappello, "Bifurcation in the MHD behaviour of a self-organizing system: The Reversed Field Pinch (RFP)," Plasma Phys. Controlled Fusion **46**, B313 (2004).
[51]L. Spitzer, *Physics of Fully Ionized Gases*, Dover Books on Physics (Dover Publications, 1956).
[52]N. Vivenzi, G. Spizzo, M. Veranda, D. Bonfiglio, S. Cappello, and RFX-mod Team, "Kinematic viscosity estimates in reversed-field pinch fusion plasmas," J. Phys.: Conf. Ser. **2397**, 012010 (2022).
[53]M. Puiatti, P. Scarin, G. Spizzo, M. Valisa, M. Agostini, A. Alfier, A. Canton, L. Carraro, E. Gazza, R. Lorenzini, R. Paccagnella, I. Predebon, D. Terranova, D. Bonfiglio, S. Cappello, R. Cavazzana, S. D. Bello, P. Innocente, L. Marrelli, R. Piovan, P. Piovesan, F. Sattin, and P. Zanca, "High density physics in reversed

field pinches: Comparison with tokamaks and stellarators," Nucl. Fusion **49**, 045012 (2009).
[54]S. Cappello, D. Bonfiglio, D. F. Escande, S. C. Guo, A. Alfier, and R. Lorenzini, "The Reversed Field Pinch toward magnetic order: A genuine self-organization," AIP Conf. Proc. **1069**, 27–39 (2008).
[55]R. Fitzpatrick, "Bifurcated states of a rotating tokamak plasma in the presence of a static error-field," Phys. Plasmas **5**, 3325–3341 (1998).
[56]Y. L. Ho, D. D. Schnack, P. Nordlund, S. Mazur, H. Satherblom, J. Scheffel, and J. R. Drake, "Effect of aspect ratio on magnetic field fluctuations in the reversed-field pinch," Phys. Plasmas **2**, 3407–3411 (1995).
[57]G. Spizzo, G. Pucella, O. Tudisco, M. Zuin, M. Agostini, E. Alessi, F. Auriemma, W. Bin, P. Buratti, L. Carraro, R. Cavazzana, G. Ciaccio, G. De Masi, B. Esposito, C. Galperti, S. Garavaglia, G. Granucci, M. Marinucci, L. Marrelli, E. Martines, C. Mazzotta, D. Minelli, A. Moro, M. E. Puiatti, P. Scarin, C. Sozzi, M. Spolaore, O. Schmitz, N. Vianello, and R. White, "Density limit studies in the tokamak and the reversed-field pinch," Nucl. Fusion **55**, 043007 (2015).
[58]P. Scarin, M. Agostini, G. Spizzo, M. Veranda, P. Zanca, and the RFX-Mod Team, "Helical plasma-wall interaction in the RFX-mod: Effects of high-n mode locking," Nucl. Fusion **59**, 086008 (2019).